Feasibility of Locating Tumours in Lung via Kinesthetic Feedback

Greig L. McCreery
Ana Luisa Trejos
Michael D. Naish
Rajni V. Patel
Richard A. Malthaner

Abstract

Background

Localizing lung tumours during Minimally Invasive Surgery is difficult since restricted access precludes manual palpation, and pre-operative imaging cannot map directly to the intra-operative lung. This study analyzes the force sensing performance that would allow an instrumented kinesthetic probe to localize tumours based on stiffness variations of the lung parenchyma.

Methods

Agar injected into ex-vivo porcine lungs produced a model approximating commonly encountered tumours. Force-deformation data were collected from multiple sites at various palpation depths and velocities, before and after the tumours were injected.

Results

Analysis showed an increase in force after the tumours were injected, ranging from 0.07 to 0.16 N at 7 mm, $p < 10^{-4}$. A 2 mm/s palpation velocity minimized exponential stress decay at constant depths, facilitating easier comparisons between measurements.

Conclusion

A sensing range of 0 to 1 N, with 0.01 N resolution should allow a kinesthetic palpation probe to resolve local tissue stiffness changes that suggest an underlying tumour.

1 Introduction

Minimally Invasive Surgery (MIS) is a surgical method which, due to its numerous advantages over conventional open surgery, is being adapted to many surgical techniques. Some of the advantages include a lower chance of infection, and reduced tissue trauma and post-operative pain [1]. Economic advantage has also been cited as a benefit of MIS, due to reduced recovery time in hospital and a faster return to work [2, 3]. These advantages are a result of the much smaller incisions, typically less than 10 mm in length, that are necessary to gain access to the surgical site.

Irrespective of the advantages, some tasks in MIS are currently more difficult to perform than in the corresponding open procedure, possibly resulting in longer operative time and thereby offsetting some of the cost-savings and potential wait-time improvements. Some of the difficulties in MIS arise

from reduced dexterity, poor ergonomic posture for the surgeon, lack of hand-eye coordination due to the reversal of lateral movements caused by pivoting about the port of entry, and the inability of the surgeon to directly manipulate the tissue [4]. Any interactions between the tissue and the instrument are difficult to perceive due to friction and mechanical moments introduced at the trocar (a protective sleeve inserted into the entry port) which tends to mask any tactile cues of the tissue interaction.

Advances in robot-assisted MIS have eliminated many of the potential drawbacks. The da Vinci® Surgical Robot (Intuitive Surgical Inc.) dramatically improves dexterity and ergonomics through the use of two 7 degree-of-freedom (DoF) articulating wrists which mimic motions at the surgeon's control console. This re-establishes direct hand-eye coordination by eliminating reversed tool motions and can present additional advantages such as motion scaling and tremor filtering [5]. Nevertheless, the loss of tactile cues remains a major drawback of MIS.

Tactile perception is an invaluable tool for many surgical procedures since it can provide rich information on the mechanical properties of the tissue being manipulated. Since a malignant tumour will typically be stiffer than the surrounding parenchyma [3], a surgeon can usually localize a tumour via direct palpation when performing open surgery. Considering the resection of a lung tumour using an MIS method, the surgeon must locate the tumour without relying on direct palpation. The common practice is to use standard MIS instruments to probe the surface of the lung, using any visual or limited tactile cues to determine the position of the tumour. If available, MIS ultrasound can be used. However, due to the poor image quality and artifacts caused by residual air in the lung, it is not usually possible to find tumours smaller than 1 cm in diameter. If the tumour cannot be located, the surgeon must increase the size of the incision and spread the ribs to allow finger access for direct palpation.

Other imaging modalities are no better suited to locating a lung tumour intra-operatively. Pre-operative Magnetic Resonance Imaging (MRI) or Computed Tomography (CT) imaging are used to identify the region of the lung in which the tumour is located, but cannot be mapped directly to the intra-operative site due to the deformability of the lung and its ability to move within the thoracic cavity. Since these imaging modalities are not commonly available in the operating room, their use as an intra-operative method of lung tumour localization is limited.

In view of these limitations, it is clear that an alternative method for locating tumours within the lung parenchyma would improve the likelihood that a lung tumour resection can be completed using minimally invasive techniques, thereby providing all of the associated benefits. One such method, which has been the subject of considerable research, is the recreation of haptic cues, or the "sense of touch," from the tissue-instrument interaction to the surgeon-instrument interface. Haptic information can be considered in two distinct modes: kinesthetic and tactile information [6].

Tactile information includes the sensation of surface textures, or distributed pressures acting across the contacting surface. Measuring tactile information requires a tightly packed array of sensors capable of measuring multiple contact pressures or forces concurrently. The use of tactile sensors to identify pulmonary lesions was discussed in [7]. Validation tests using a foam model showed promising results. Tactile feedback systems have also been proposed for identification and characterization of lesions in the breast [8] and for identifying arteries during robotic surgery [9].

In contrast to tactile information, which requires a dense cluster of sensors, kinesthetic information relates to the movement and bulk forces acting in the joints of an arm (human or mechanical) and at the point of contact. Kinesthetic information may be used to assess the contour and stiffness of an object and may be acquired using a simple force/torque sensor. Numerous researchers have proposed using kinesthetic feedback to measure force and displacement during an MIS procedure for various purposes. In [5], a 6 DoF force/torque sensor based on a strain gauge instrumented Stewart's

platform is proposed. The sensor is steam sterilizable and small enough to pass through a standard trocar. Therefore, it can be located at the distal end of the instrument where trocar imposed friction and moments will not interfere with the tissue interaction measurements. The sensor is designed for use with a grasper system, and is capable of achieving a force resolution of 0.25 N in the z-direction and 0.05 N in the x- and y-directions. This sensor system is intended for use in a robotic surgical system to help reduce unintentional damage to tissue and suture material by the inadvertent application of excess force. A 3 DoF force sensor intended for the same purpose, but based on fiber-optic sensing, is presented in [10]. The prototype exhibited a sensing resolution of 0.04 N.

A strain gauge sensorized laparoscopic grasper was developed in [11]. The grasping force and grasper position were presented along with a measure of compliance, which could be used to differentiate between objects of various stiffnesses. Another instrumented grasper, utilizing 2 thin foil strain gauges, is described in [3]. This system is capable of operating in a wet saline environment due to silicone encapsulation of the electronics, and can determine the location of the applied force along the grasper jaws. The sensitivity can be adjusted by varying the amplifier gain, and the system was reported to be sensitive to a force increase of "a few grams." It was also shown through Finite Element Analysis that the system could be used to measure distributed forces, approximating them as a concentrated load. A computerized endoscopic surgical babcock grasper that utilizes existing surgical tools is described in [12]. It performs an automatic palpation consisting of 3 cycles of a 1 Hz sinusoidal displacement of the grasper. Experimental results indicating the tool's ability to distinguish different mechanical properties of tissues appear promising. In [13] tissue interaction was measured using a number of strain gauges and a single-axis load cell integrated into a custom endoscopic instrument. A different approach is used in [14], in which tissue stiffness is determined by measuring the amount of current applied to the motor of a motorized grasper.

For the purposes of medical diagnosis, instrument design and improved simulations, *in-vivo* and *ex-vivo* indentation testing of human and porcine abdominal organs was presented in [15]. It was claimed that this included possibly the first *in-vivo* measures of tissue compliance from a human subject. The results indicated that the stiffness between healthy liver tissue does not vary widely, but that a diseased liver with an obstructed bile duct demonstrated a notable difference in compliance. It was therefore suggested that an indentation testing instrument similar to that used in the study could be used during MIS as a diagnostic tool.

To the best of our knowledge, the use of kinesthetic feedback from direct probing using a sensorized instrument, rather than grasping, has not been applied to the task of tumour localization within the lung. For this task, a probe instrument may be better suited than a grasper since it may be difficult to reach all parts of the lung, or to fully capture the tumour when using a grasper instrument. It is hypothesized that the force measured will be higher when probing tissue with an underlying tumour than when probing intact tissue at the same depth.

The goal of this paper is threefold: 1) to determine with statistical confidence that the measurements from indentation testing can indicate the presence of a tumour; 2) from the testing methods used, to determine which performed the best in terms of measured force increase due to a tumour while minimizing the number of false negative results; and 3) to determine the sensing range and resolution that is required to realize the approach in actual MIS.

The design of a sensor system for accurately measuring the tissue-tool interactions in an MIS setting presents considerable challenges in that the sensor must meet demanding size constraints, withstand temperature variations, address issues of sterilization, and use biocompatible materials, while achieving appropriate performance in terms of resolution and sensing range. While these constraints were not addressed by the system used in these experiments, the results will be useful in providing target design

specifications for systems which address such constraints.

2 Methods

2.1 The Model

In order to experimentally verify that kinesthetic feedback alone could indicate the presence of a tumour in lung parenchyma, an accurate model was required. *Ex-vivo* porcine lung tissue was collected from local abattoirs and used as a biological model for human lung. When not in use, the lungs were individually sealed in plastic bags containing approximately 300 mL of saline and refrigerated. To minimize the effects of autolysis of the tissue, all experiments were completed within 60 hours *post-mortem*.

Several preliminary tests were undertaken to determine the most realistic method of simulating tumours [16]. It was discovered that any method which required a major incision in the tissue changed the force-deformation behaviour of the otherwise intact lung. Therefore, injecting material provided the most realistic alternative. Sigma Gelrite Gellan Gum (agar) was prepared in a ratio of 225 mL water to 7.5 g agar, boiled, and injected into the cold lung. Given that the tumours of interest were approximately 1 cm in diameter, 0.5 mL of the agar preparation should have been injected. However, initial tests revealed that the tumours formed were not perfectly spherical, and that some of the liquid agar was lost through the injection puncture. Therefore, approximately 1.5 mL was used to form each tumour. A sample of the artificial tumours, excised after testing was completed, is shown in Figure 1. No evidence of agar absorption into the surrounding parenchyma was noted during excision of the tumours.

Experience in thoracic surgery has shown that the tumours typically encountered in lung can span a range of stiffnesses. In qualitative terms, the feel of typical tumours commonly encountered in the operating room can be described as ranging from the stiffness of a grape to that of a rock. The agar tumours used herein fell within this range, as verified by an experienced thoracic surgeon.

In [17] it was shown that the Bulk Modulus and Young's Modulus of canine lung are proportional to the inflation pressure in the airways, being 4 times and 1.5 times higher, respectively. Currently, during MIS lung tumour resection, the lung of interest is occluded at the bronchus and collapsed. Due to the continued perfusion of the lung, most of the residual gases in the alveoli are absorbed by the pulmonary circulation. The lungs tested in the following experiments were not pressurized. Due to the elastic nature of the alveoli and terminal bronchi, it can be reasonably assumed the alveolar pressure will be either equal to, or slightly greater than, atmospheric pressure. Hence, the stiffness of the tissue will be either equal to, or slightly stiffer than that of an intra-operative lung. Since discerning a tumour in stiffer parenchyma would be more difficult due to the less marked difference in stiffnesses, the *ex-vivo* model used here represents a 'worst-case' model, compared to the intra-operative condition.

2.2 Apparatus

The kinesthetic probe was realized using an aluminum rod approximately 50 cm long with a diameter of 9 mm and a hemispherical distal tip. A Gamma Force/Torque sensor from ATI Industrial Automation, Inc. was placed in series between the proximal end of the probe and the mounting plate of a Mitsubishi PA10-7C robot, Figure 2. The Gamma sensor was factory calibrated for 100 N measurement range in the z-direction (axial direction of the probe), and 32 N in both the x- and y-directions. The resolution is 0.003 N in the z-direction and 0.002 N in the x- and y-directions. Force data for the three orthogonal vectors was used to calculate the magnitude of the resultant force vector, from which all of the analysis

was conducted. It was assumed that using the resultant force vector would result in more robust data, since slight deviations between the normal of the lung surface and the approach vector would not affect the resultant force to the same degree as it would the axial force. Note that, for all tests conducted in this study, the end-effector orientation relative the robot base was not modified and the probe was, at all times, approximately perpendicular to the table on which the lung was tested. The effect of various approach angles was not considered.

2.3 Experimental Approach

Using kinesthetic feedback to measure a change in stiffness can be accomplished in two ways: The tissue can be indented until a pre-set force is achieved, and the depth is recorded; or, the tissue is indented to a specific depth from the surface, and the force is recorded. This question was examined both experimentally and analytically in [18], where it was found that the constant depth scheme is more sensitive to stiffness deviations when testing visco-elastic materials with an upward-sloping, non-linear deformation curve. Therefore, the constant depth method was adopted for this study.

The lung sample was placed on a surgical towel which was clamped onto a fibreglass tray, thereby preventing lateral movement of the lung during testing. The mounted sample was placed within the robot workspace, with the probe aligned above the first palpation point.

The robot was programmed to move down, in a direction parallel to the long axis of the probe, toward the surface of the lung in 0.5 mm increments until a threshold force of 0.04 N was detected in the axial direction. This threshold was shown to be the smallest value that was not prone to frequent false triggers due to the inertial forces of the probe. Once the threshold value was realized, the robot was held stationary, during which time 17 measurements were recorded at a sampling rate of 250 Hz. If the median of these measurements was greater than the 0.04 N threshold, the operator was prompted to confirm that the probe was indeed in contact with the surface of the lung. This redundant process was used to avoid "false starts" which occurred during preliminary tests that used only a single measurement of the threshold value.

Once it was confirmed that the probe tip was just in contact with the surface of the tissue, a 10 second acquisition of continuous force measurements in three orthogonal directions was initiated at a sampling rate of approximately 250 Hz. The probe was then advanced into the lung tissue to a pre-programmed depth: either 5, 7 or 9 mm, after which it was held stationary for the remainder of the 10 second sampling period. Once the measurement was complete, the probe was retracted to a position above the lung, and moved to a point on the lung 30 mm away from any previous testing site and the palpation process was repeated. Pre-planning of the testing grid ensured that only the lower lobe was sampled, and that the main bronchial branches were avoided. After testing was completed for each lung, a permanent marker was used to mark each palpation site on the surface of the lung.

Once all initial tests were completed for a specific depth, the agar was prepared and 1.5 mL were injected into each palpation site, to approximately the mid-thickness of the lung. The palpation tests were then repeated. Radiographs of the lung, such as that shown in Figure 3, revealed that since the tumours occasionally did not form directly beneath the intended site, each tumour needed to be located using manual palpation and aligned with the probe prior to testing. The test sites were numbered such that the measurements from before and after the tumour was injected could be paired for each location.

Before the data were analyzed, some measurements from either the test or control lungs were removed because the operator had noted an error in the measurement process. Errors included inadvertently testing extremely thin or damaged regions of the lung. Note that the data analysis was blinded from the acquisition of the data, and any trials that were indicated to be questionable were

removed without reviewing the results. After all questionable samples were removed, over 30 samples for each depth remained.

Since the indentation velocity will affect the force-deformation behavior of a visco-elastic material, the above mentioned experiments were performed with two variations of velocity control. In the variable-velocity approach, the maximum velocity of the robot was left as the default of 40 mm/s. Because of the short translations required in the palpation experiment, this velocity was not reached. However, from preliminary experiments it was evident that the peak velocity increased with palpation depth. Therefore, velocities could be considered equal when comparing uniform depths, but not between depths. For the constant-velocity approach, the maximum velocity was set to 2 mm/s. Since this velocity was attainable at all palpation depths tested, comparisons at constant velocity could be made across all depths.

2.4 Pre-Conditioning and Experimental Controls

Over repetitive strain cycles, the response of soft tissue approaches a steady state stiffness and hysteresis. This effect is known as pre-conditioning [19], and is commonly employed in tissue research to obtain more consistent results. In [19], *in-vivo* and *in-situ* tissue did not tend to reach a pre-conditioned state within 10 cycles. Since tissue is not normally pre-conditioned during actual surgery, the number of measurements taken at each point was minimized to reduce the pre-conditioning effect. At each test site, only one sample was collected for the intact tissue, followed by a single sample after the agar had been injected. Furthermore, test sites were placed at least 30 mm apart, thereby reducing the influence from an adjacent test site. In total, 38 pairs of lungs were tested.

In [19], the differences in the force-deformation relationship between *in-vivo* and *in-situ* were examined, indicating that the stress-relaxation and tissue recovery differed between the samples. Additionally, [20] indicates that tissue properties can change by as much as 50% when comparing *in-vivo* to *ex-vivo* samples, and that level of hydration, time *post-mortem*, temperature and tissue perfusion all affect the visco-elastic properties of the tissue.

In order to isolate the changes that were caused by the presence of the artificial tumour from changes caused by tissue autolysis[1] and other environmental factors, tissue controls were incorporated into the testing. When the lungs were excised, the right and left lung remained connected by the intact portion of the bronchi. In all cases, the left lung was used as the test lung with tumour injected, while the right lung was used as the control. Both lungs were exposed to the same environmental conditions and treatment, with the exception that no artificial tumours were injected into the control lungs. Since the lungs came from the same animal and remained connected throughout the experiments, the effect of factors such as time *post-mortem*, temperature cycles, hydration, etc., could be isolated from the effect of the artificial tumour. Again, the test sites were numbered, such that the resulting measurements at each location could be paired.

2.5 Signal Conditioning

Continuous force measurements were collected for 10 seconds at a sampling rate of approximately 250 Hz. The raw data were post-processed in MATLAB using the *filtfilt* function and a second order Butterworth filter with a cutoff frequency of approximately 2.9 Hz, as no high frequency signal was expected. This filtering scheme filters the raw data in the forward direction, and then re-filters the output in the reverse direction. This eliminates any phase distortion and also serves to effectively

[1]The enzymatic digestion of cells by enzymes present within them.

double the order of the filter [21]. Figure 4 shows the raw and filtered data from two palpation tests at 9 mm, using both the variable- and constant-velocity approach.

2.6 Peak vs. Settled Measurements

Since lung tissue tends to exhibit a well known decaying stress with constant strain, as can be seen in Figure 4, it is important that any comparisons between measurements be made at the same point on the curve. Two points were considered in this study: the peak force measured, and the force after the response had settled, taken at a constant number of data points from the peak. This was determined separately for each of the six combinations of depth and velocity control approaches.

For each experimental approach, the number of data points from the peak to the end of the measurement window was determined for each sample in the set, and the mean calculated. The minimum of these values was set as the number of data points from the peak to where the settled measurements would be read. However, since some samples exhibited an uncharacteristic peak near the end of the measurement window, samples where this value deviated by more than 3 standard deviations from the mean were permanently removed from further evaluation to avoid skewing the read time of the settled value. To mitigate the influence of noise on the settled value, the median of the 201 data points prior to the identified target measurement was reported as the settled value.

3 Results

Each of the experiments outlined in Section 2 were performed in a paired manner, assessing the response of the lung tissue before and after a tumour was introduced. Three different palpation depths were considered with the probe advancing under both variable- and constant-velocity schemes. These tests resulted in 6 data sets: 5 mm variable-velocity, 7 mm variable-velocity, 9 mm variable-velocity, 5 mm constant-velocity, 7 mm constant-velocity and 9 mm constant-velocity. Futhermore, the peak and settled force for each sample were determined following the methodology outlined in Section 2.6, effectively doubling the number of data sets. In addition, each lung had an associated control (in which agar was not injected), where each site was also tested twice, yielding an additional 12 data sets. The aggregate data from these 24 data sets was used to assess the maximum observed forces and the observed force difference within paired palpations (pre- and post-tumour injection).

3.1 Maximum Force Measurements

For the purpose of defining an appropriate sensor range for a kinesthetic lung tumour localization system, it is necessary to look at the maximum forces occurring in each of the experimental approaches. For this purpose, the peak measurement from each artificial tumour test, as determined in Section 2.6, is shown in Figure 5.

3.2 Tissue Controls and Unadjusted Tumour Test Results

For both the artificial tumour tests described in Section 2.3 and control tests outlined in Section 2.4, the change in force feedback given by $\Delta F = F_f - F_i$ was determined for each pair of samples, where F_f is the measurement recorded with the tumour present, or the second test of the control; and F_i is the force measured during the initial palpation of either the test or control lung. These ΔF values were grouped into sets according to depth, velocity scheme and peak or settled values. The results are plotted as box plots and presented for the variable-velocity peak and settled, and constant-velocity

peak and settled sets in Figures 6–9, respectively. Within each set, the tumour test data is adjacent to the corresponding control data for each depth.

The upper and lower bound of the box plot represents the first and third quartile of the measurements. The line through the box represents the median, while the notch represents the range of the 95% confidence interval of the median of the samples. If the notches of two sample sets do not overlap, it can be concluded with 95% confidence that the true medians do differ. The whiskers represent the range of measurements not including outliers, which are defined as measurements deviating from the median by more than 1.5 times the interquartile range and are indicated by a '+'.

All p-values, determined using the *Mann-Whitney Independent Sample Test*, were less than 10^{-6}. This non-parametric test is analogous to the *two-sample independent t-test*, but is applicable when the assumptions of normal distribution, implicit in the use of the *two-sample t-test*, cannot reasonably be made [22]. All statistical analysis was performed using the MATLAB® Statistical Toolbox, and verified using SPSS.

3.3 Artificial Tumour Data, Adjusted for Controls

Before the results from the artificial tumour tests (see Section 2.3) can be interpreted, any changes that can be attributed to factors other than the presence of a tumour must be accounted for. For each test-control pair (see Section 2.4), the value of the upper quartile measurement of the control was used to offset the tumour test data to account for these changes. The resulting tumour test data, corrected for the controls, are shown for variable-velocity peak and settled and constant-velocity peak and settled sets in Figures 10–13, respectively. Within each figure, the percentage of *negative* differences (i.e., the second force measurement was less than the initial measurement) and the total sample size is indicated for each sample set.

For this analysis, p-values were determined using the *Wilcoxon Paired-Sample Test*, and found to be less than 10^{-4} in all cases. This non-parametric test is analogous to the *paired-sample t-test*, but again, is valid when assumptions of normal distribution and equal variance cannot be made.

4 Discussion

4.1 Control Validation

Examining the response of the controls in Figures 6–9, reveals that there was some change in the force-deformation characteristics of the lungs which were not associated with the presence of the artificial tumours. Factors such as temperature variations, tissue autolysis, hydration fluctuations, tissue conditioning effects from the first palpation test, manipulation of the lung, or measurement error may have contributed to these deviations. There is no discernable trend for this change across the various palpation depths.

The p-values determined for the *Mann-Whitney test* provide a very positive statistic that the tumour test results and control test results are different. This supports the methodology that assumes there is some change in the force-deformation behaviour of the lung that can be directly attributed to the artificial tumour.

By shifting the tumour test data sets toward zero by an amount equal to the upper quartile measurement of the associated control response, the corrected data in Figures 10–13 provide a more realistic indication of the force feedback deviations that can be expected in the presence of a tumour.

4.2 Statistical Analysis of the Proposed Method

It is clear from the corrected test results in Figures 10–13, that each experimental approach performed reasonably well. The *Wilcoxon Paired-Sample Test* analysis indicates that regardless of velocity-control schemes or measurement time, each approach produced a statistically significant change in the force-deformation behaviour in the presence of a tumour, with all p-values being less than 10^{-4}. This provides a statistical indication that kinesthetic feedback alone could be used to detect these tumours within lung tissue. However, some methods appeared to be consistently better than others.

The percentage of *negative* force differences provides an indication of the likelihood of arriving at a false negative conclusion (i.e., not seeing a force *increase* in the presence of a tumour). Again, the 7 mm palpation tests consistently produced the least number of false negatives when testing the variable-velocity approach. The 7 and 9 mm palpations both resulted in 3% negative force differences when the peak force of the constant-velocity approach was analyzed, whereas the false negatives resulting from the 7 mm palpation increased to 7% when considering the settled values. However, it should be noted that the negative value causing this change was extremely close to zero, of the order -10^{-3}. If this value were assumed to be zero, the percentage of false negatives for the 7 mm test would again fall to 3%. Furthermore, in an operative setting, multiple palpations by the surgeon may mitigate the effect of false negative results.

Finally, the 7 and 9 mm constant-velocity palpation tests produced very similar performance in terms of the median force difference measured, ranging from 0.12 to 0.13 N. While the medians were very similar, the data spread tended to be tighter for the 7 mm tests and the false negatives were a result of outlier measurements. The tighter data spread provides a more precise indication of the force increase that would be associated with a tumour, and may allow a more accurate conclusion regarding the presence of an underlying tumour. The greatest median ΔF overall was a result of the 9 mm variable-velocity test. However, this approach was also associated with the highest incidence of false negative results.

The median force difference for the 5 mm palpation tests was lower than the 7 mm and 9 mm tests regardless of measurement or analysis method. This indicates that while the 5 mm palpation tests produced a reasonable test statistic, it was not optimal in any of the experimental approaches. It is interesting to note that the data spread is minimal for all 5 mm tests compared to the other depths. Presumably, the shallower palpation depth would not be influenced by a rigid support medium to the same extent as deeper palpations. This is especially significant in thinner regions of the lung, where deeper palpation depths might exhibit an altered response due to the underlying rigid support surface.

4.3 Effect of Velocity

If the deviations observed with differing palpation velocity are due to the visco-elastic nature of the tissue, it would follow that once the tissue had settled, there should be little difference between the response of the variable- and constant-velocity tests, at the same palpation depth. By comparing Figures 11 and 13, it is clear that the median of the settled responses for the variable- and constant-velocity tests cannot be concluded to be different at a 95% confidence level. This suggests that any difference in the measured peak response that is attributed to a higher palpation velocity, tends to diminish as the sample settles.

Furthermore, comparing the peak and settled values between the two velocity schemes, it can be seen that the 95% confidence interval of the median peak and settled values tend to have a greater overlap when considering the constant-velocity (or slower) approach. This indicates that when using the slower palpation approach, reasonably accurate comparisons could be made from readings taken

after different settling times have elapsed. The nearly-constant stress resulting from the constant-velocity approach shown in Figure 4 illustrates this well. This may be advantageous when considered in a clinical setting, where maintaining a constant strain for an extended period may not be possible. When considering the faster, variable-velocity approach, the pronounced peak and decaying strain imply that to make comparisons between two tests, the time at which the response is analysed is critical.

4.4 Experimentally Determined Range and Resolution Required

The peak values shown in Figure 5 are the maximum forces that were recorded when testing each site after a tumour had been injected. This gives a good indication of the maximum forces that can be expected during the use of a kinesthetic instrument to locate a tumour in the lung.

With the exception of a few outliers, the peak measurements are less than 2 N and 1 N for the variable-velocity and constant-velocity tests, respectively. Thus, it would be reasonable to define the full scale range of a sensor system as 0 to 2 N; or 0 to 1 N, depending on the palpation velocity being used.

The required resolution can be determined from the corrected ΔF values given in Figures 10–13. Since the 7 mm constant-velocity approach appeared to perform slightly better than the 9 mm, the values from this method, considering both the peak and settled analysis, will be considered in determining the required resolution.

Considering the upper and lower quartile bounds from both the peak and settled analysis, a significant portion of the ΔF values range from 0.07 to 0.16 N. Therefore, if a MIS kinesthetic sensing system in unable to resolve force differences within this range, it would not likely be able to differentiate the majority of these underlying tumours. Even a solution capable of resolving differences in force as small as 0.07 N would result in false negative results in 25% of these tests. It should be noted that in a clinical situation, multiple palpations around the suspected area would likely be employed. This approach, combined with the currently available visual cues and limited tactile feedback transmitted through the rigid instrument, may tend to reduce the likelihood of arriving at a false negative conclusion.

In order to resolve the desired force differences, the resolution of the instrument should be one order of magnitude less than this value, to avoid quantization error. Thus, a sensor resolution of 0.007 N, or approximately 0.01 N is suggested.

5 Conclusion

This study was performed to determine if there was a statistically significant difference in force-deformation behaviour between intact lung tissue and tissue in which a lesion was present, using *ex-vivo* porcine lung with injected agar simulating the tumours. The differences observed were used to suggest an acceptable sensing range and resolution, and an appropriate palpation velocity, that may allow a kinesthetic feedback instrument to be used to locate tumours in the lung during a minimally invasive procedure.

Control tissues were used to quantify, and correct for, any change in the force-deformation behavior of the tissue that may not have been due to the insertion of a tumour. The control lungs were from the same animals and were exposed to the same environmental conditions and handling as the test lungs, with the exception of the agar injection. Any statistically significant change that was observed in the control was used to correct the tumour test measurements.

Tests were conducted using a constant 2 mm/s palpation velocity across all palpation depths, as well as using a variable-velocity approach in which the peak velocity increased with palpation depth. The slower, constant-velocity approach appears to be superior since the exponential stress decay tends to be significantly diminished compared to that in the variable-velocity approach. Thus, comparisons can more accurately be made between measurements collected at any time after the desired palpation depth has been reached.

Of the palpation depths tested, being 5, 7 and 9 mm, the 7 mm constant-velocity tests tended to perform the best, in terms of statistical confidence in the observed force increase, the limited data spread, and the number of false negative results. However, the performance of the 9 mm constant-velocity approach was very similar to the 7 mm, with the exception of a wider data spread. Both the 7 and 9 mm constant-velocity approaches were clearly superior to the other methods tested.

It must be noted that even using the most successful approach, as much as 7% of the tests exhibited no quantifiable increase in stiffness in the presence of a tumour, indicating that a false negative conclusion would be inevitable in some cirumstances, regardless of resolution of the instrument. Nonetheless, the use of a kinesthetic feedback system in a clinical setting could be enhanced by the limited visual and tactile cues that are currently available, possibly reducing the likelihood of false negative conclusions. Furthermore, multiple palpations of suspected sites would also serve to reduce the likelihood of incorrect results.

The peak forces and differences in force-deformation behavior observed, and corrected for by the control values, suggest that a full scale sensing range of 0 to 1 N would be appropriate for a kinesthetic feedback instrument intended for use in lung tumour localization. To avoid quantization error, an instrument with a minimum resolution of 0.01 N is required.

6 Future Work

The results from this study will assist in defining suitable operating characteristics for sensors used to identify the location of lung tumours. Future work involves the development of clinical instruments that use kinesthetic feedback for tumour localization in MIS.

7 Acknowledgments

The authors would like to thank the following individuals whose assistance was invaluable in the realization of this study: Sheri VanLingen for her assistance in acquiring the test specimens, Dave Browning and Dave Harrison for their help with the experimental set-up, Shiva Mohan for his support with the data acquisition system, and Chris Kong for his assistance in the experimentation.

References

[1] Lanfranco AR, Castellanos AE, Desai JP, Meyers WC. Robotic Surgery: A Current Perspective. Annals of Surgery. 2004;239(1):14–21.

[2] Cuschieri A, Berci G. Laparoscopic Biliar Surgery. Oxford, UK: Blackwell Scientific Publications; 1993.

[3] Dargahi J. An Integrated Force-Position Tactile Sensor for Improving Diagnostic and Therapeutic Endoscopic Surgery. Bio-Medical Materials and Engineering. 2004;14(2):151–166.

[4] Camarillo DB, Krummel TM, Salisbury JK. Robotic Technology in Surgery: Past, Present, and Future. The American Journal of Surgery. 2004 Oct;188:2S–15S.

[5] Seibold U, Kubler B, Hirzinger G. Prototype of Instrument for Minimally Invasive Surgery with 6-Axis Force Sensing Capability. In: Proceedings of the IEEE International Conference on Robotics and Automation. Barcelona, Spain; 2005. p. 496–501.

[6] Ottermo MV, Ovstedal M, Lango T, Stavdahl O, Yavuz Y, Johansen TA, Marvik R. The Role of Tactile Feedback in Laparoscopic Surgery. Surgical Laparoscopy, Endoscopy & Percutaneous Techniques. 2006;16(6):390–400.

[7] Miller AP, Peine WJ, Son JS, Hammoud MD. Tactile Imaging System for Localizing Lung Nodules During Video Assisted Thoracoscopic Surgery. In: Proceedings of the IEEE International Conference on Robotics and Automation. Roma, Italy; 2007. p. 2996–3001.

[8] Wellman PS, Howe RD. Extracting Features From Tactile Maps. In: Proceedings of the Second International Conference on Medical Image Computing and Computer-Assisted Intervention. Cambridge, UK: Springer-Verlag; 1999. p. 1133–1142.

[9] Beasley RA, Howe RD. Tactile Tracking of Arteries in Robotic Surgery. In: Proceedings of the IEEE International Conference on Robotics and Automation. vol. 4. Washington, DC; 2002. p. 3801–3806.

[10] Peirs J, Clijnen J, Reynaerts D, Van Brussel H, Herijgers P, Corteville B, Boone S. A Micro Optical Force Sensor for Force Feedback During Minimally Invasive Robotic Surgery. Sensors and Actuators A: Physical. 2004;115:447–455.

[11] Bicchi A, Canepa G, De Rossi D, Iacconi P, Scillingo E. A Sensor-Based Minimally Invasive Surgery Tool for Detecting Tissue Elastic Properties. In: Proceedings of the IEEE International Conference on Robotics and Automation. vol. 1. Minneapolis, MN, USA; 1996. p. 884–888.

[12] Hannaford B, Trujillo J, Sinanan M, Moreyra M, Rosen J, Brown J, Leuschke R, MacFarlane M. Computerized Endoscopic Surgical Grasper. In: Westwood JD, Hoffman HM, Stredney D, Weghorst SJ, editors. Medicine Meets Virtual Reality 6. IOS Press; 1998. p. 265–271.

[13] Tavakoli M, Patel RV, Moallem M. Haptic Interaction in Robot-Assisted Endoscopic Surgery: A Sensorized End-effector. International Journal of Medical Robotics and Computer Assisted Surgery. 2005;1(2):53–63.

[14] Tholey G, Desai JP, Castellanos AE. Force Feedback Plays a Significant Role in Minimally Invasive Surgery: Results and Analysis. Annals of Surgery. 2005;241(1):102–109.

[15] Carter FJ, Frank TG, Davies PJ, McLean D, Cuschieri A. Measurements and Modelling of the Compliance of Human and Porcine Organs. Medical Image Analysis. 2001;5(4):231–236.

[16] McCreery GL, Trejos AL, Patel RV, Naish MD, Malthaner RA. Evaluation of Force Feedback Required for Minimally Invasive Lung Tumour Localization. In: Proceedings of the IEEE/RSJ International Conference on Intelligent Robots and Systems. San Diego, CA, USA; 2007. p. 883–888.

[17] Lai-Fook SJ, Wilson TA, Hyatt RE, Rodarte JR. Elastic Constants of Inflated Lobes of Dog Lungs. Journal of Applied Physiology. 1976;40(4):508–513.

[18] Yen PL. Palpation Sensitivity Analysis of Exploring Hard Objects Under Soft Tissue. In: Proceedings of the IEEE/ASME International Conference on Advanced Intelligent Mechatronics. vol. 2. Port Island, Kobe, Japan; 2003. p. 1102–1106.

[19] Brown JD, Rosen J, Kim YS, Chang L, Sinanan MN, Hannaford B. In-vivo and In-situ Compressive Properties of Porcine Abdominal Soft Tissues. In: Westwood JD, Hoffman HM, Mogel GT, Phillips R, Robb RA, Stredney D, editors. Medicine Meets Virtual Reality 11. IOS Press; 2003. p. 26–32.

[20] Ottensmeyer MP, Kerdok AE, Howe RD, Dawson SL. The Effects of Testing Environment on the Viscoelastic Properties of Soft Tissues. In: Proceedings of the Second International Symposium on Medical Simulation. Cambridge, MA, USA: Springer; 2004. p. 67–76.

[21] Signal Processing Toolbox 6 User's Guide. The Mathworks Inc.; 2007.

[22] Zar JH. Biostatistical Analysis. Upper Saddle River, NJ: Prentice-Hall, Inc.; 1999.

List of Figures

1 A sample of the artificial tumours excised from the lungs after testing was completed. 15
2 The Mitsubishi PA10-7C palpating an *ex-vivo* porcine lung. 16
3 Digital Radiograph of *ex-vivo* porcine lung after three agar simulated tumours were injected. The three solid black lines in the left of the image are 22 gauge needles that were inserted to mark the initial palpation site. A needle marker is also present in the bronchus. 17
4 The raw and filtered data of two 9 mm palpations: one taken from the variable-velocity scheme, and the other from the constant velocity scheme. 18
5 Peaks of all force measurements recorded with a tumour present. Both constant- and variable-velocity results are shown. 19
6 ΔF of the peak measurements from the variable-velocity experimental approach. . . . 20
7 ΔF of the settled measurements from the variable-velocity experimental approach. . . 21
8 ΔF of the peak measurements from the constant-velocity experimental approach. . . . 22
9 ΔF of the settled measurements from the constant-velocity experimental approach. . . 23
10 ΔF of the peak measurements from the variable-velocity experimental approach, corrected for the deviations in the associated control. 24
11 ΔF of the settled measurements from the variable-velocity experimental approach, corrected for the deviations in the associated control. 25
12 ΔF of the peak measurements from the constant-velocity experimental approach, corrected for the deviations in the associated control. 26
13 ΔF of the settled measurements from the constant-velocity experimental approach, corrected for the deviations in the associated control. 27

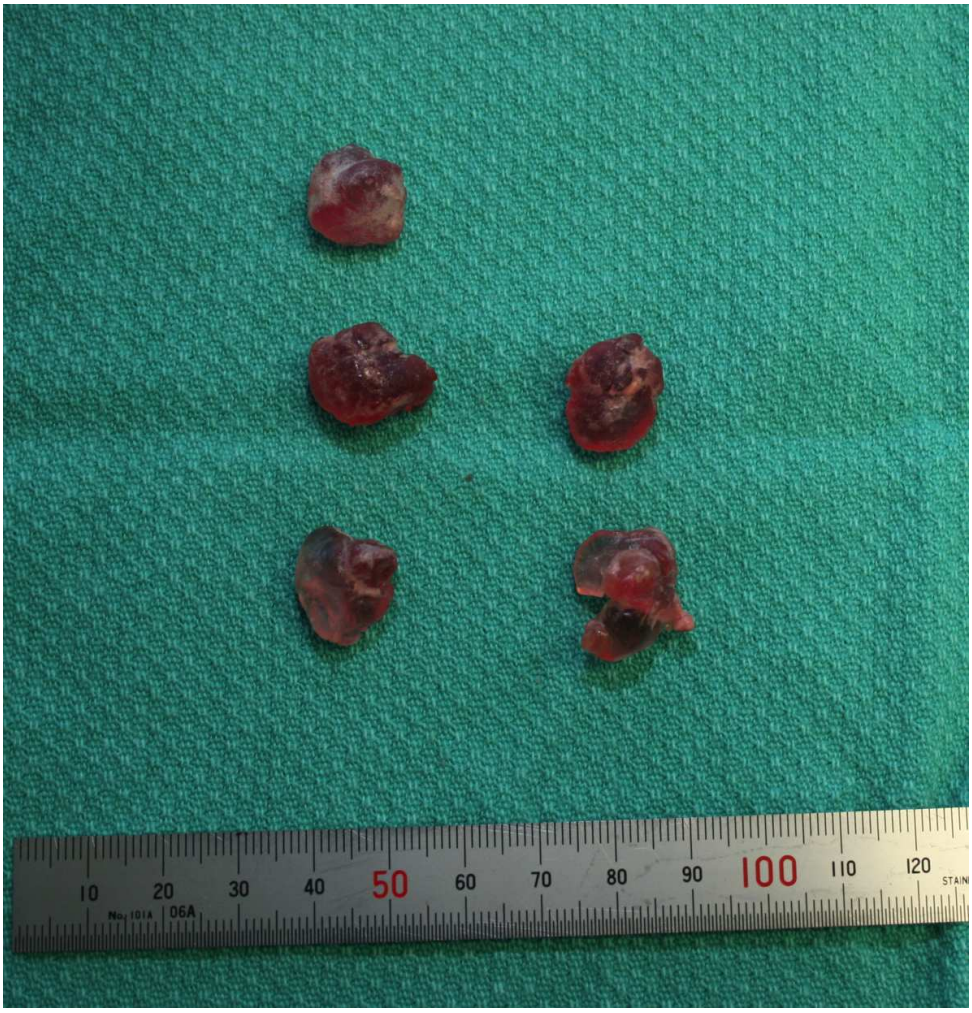

Figure 1: A sample of the artificial tumours excised from the lungs after testing was completed.

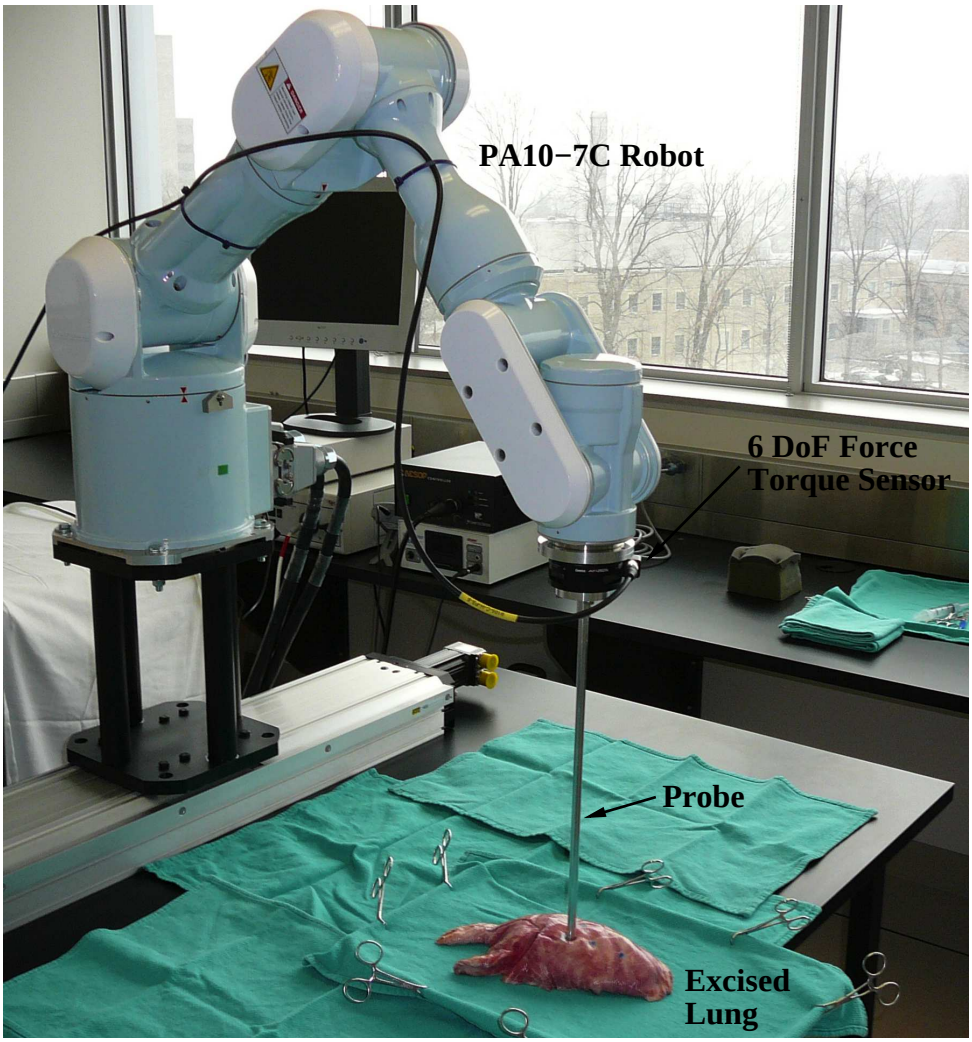

Figure 2: The Mitsubishi PA10-7C palpating an *ex-vivo* porcine lung.

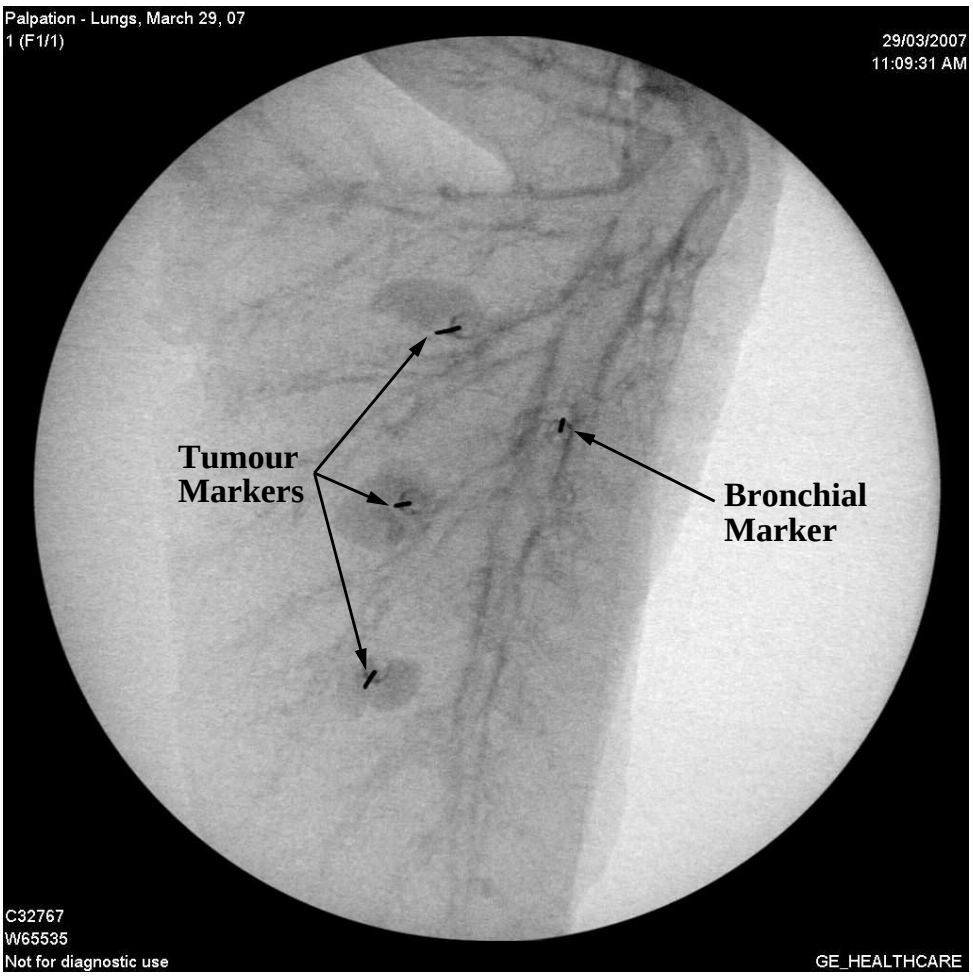

Figure 3: Digital Radiograph of *ex-vivo* porcine lung after three agar simulated tumours were injected. The three solid black lines in the left of the image are 22 gauge needles that were inserted to mark the initial palpation site. A needle marker is also present in the bronchus.

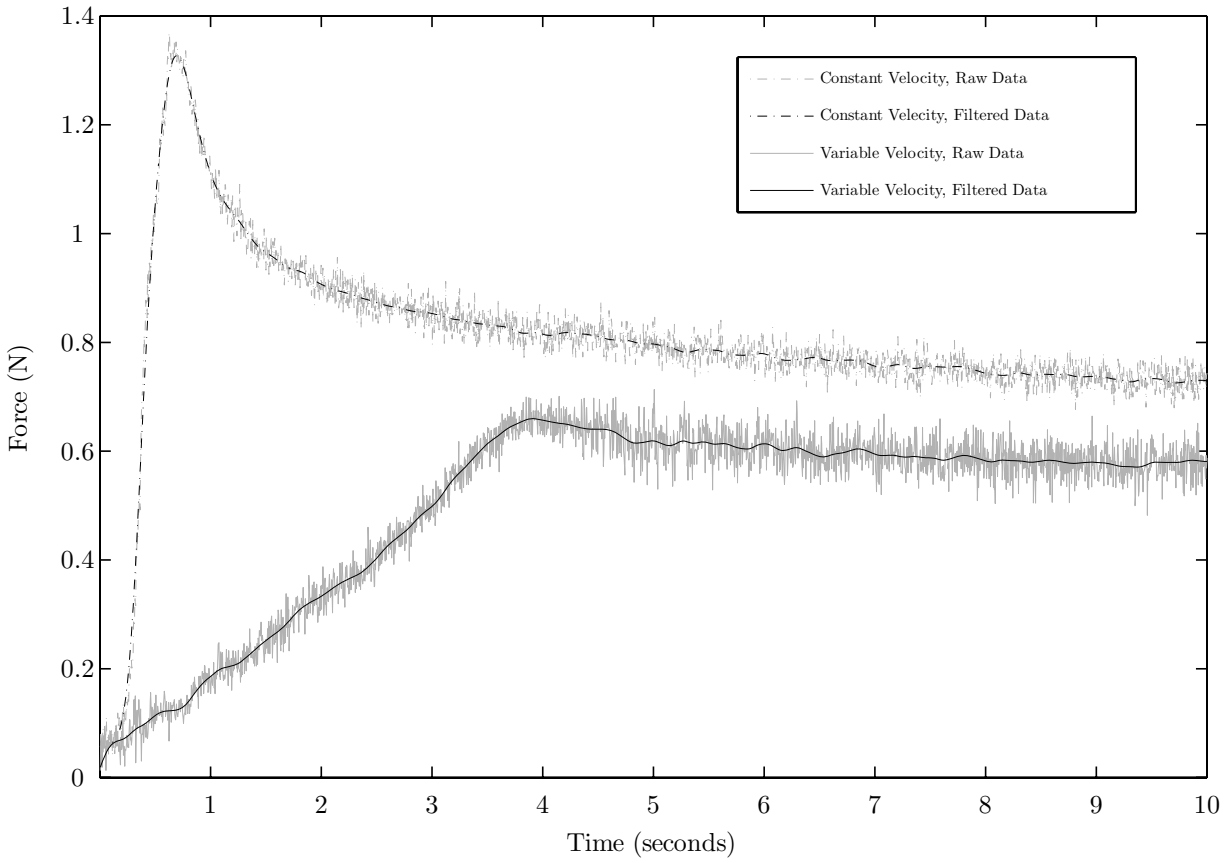

Figure 4: The raw and filtered data of two 9 mm palpations: one taken from the variable-velocity scheme, and the other from the constant velocity scheme.

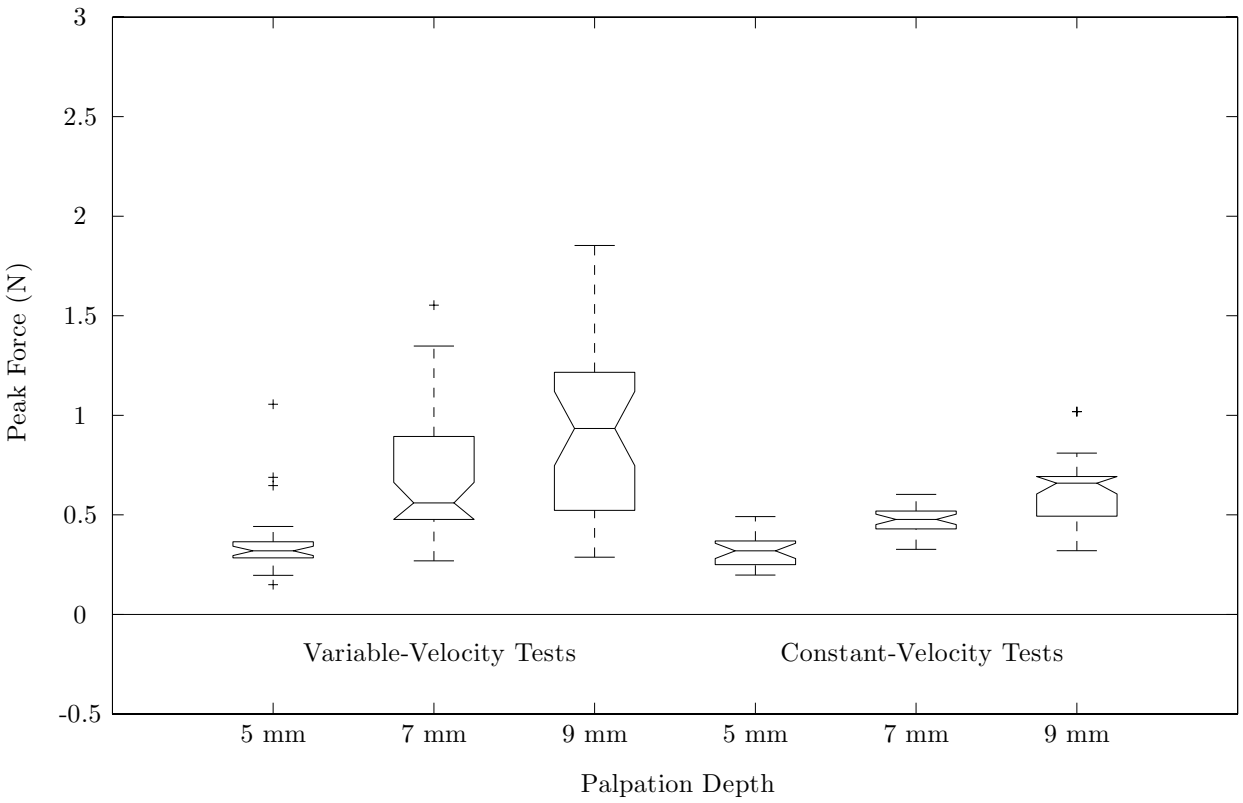

Figure 5: Peaks of all force measurements recorded with a tumour present. Both constant- and variable-velocity results are shown.

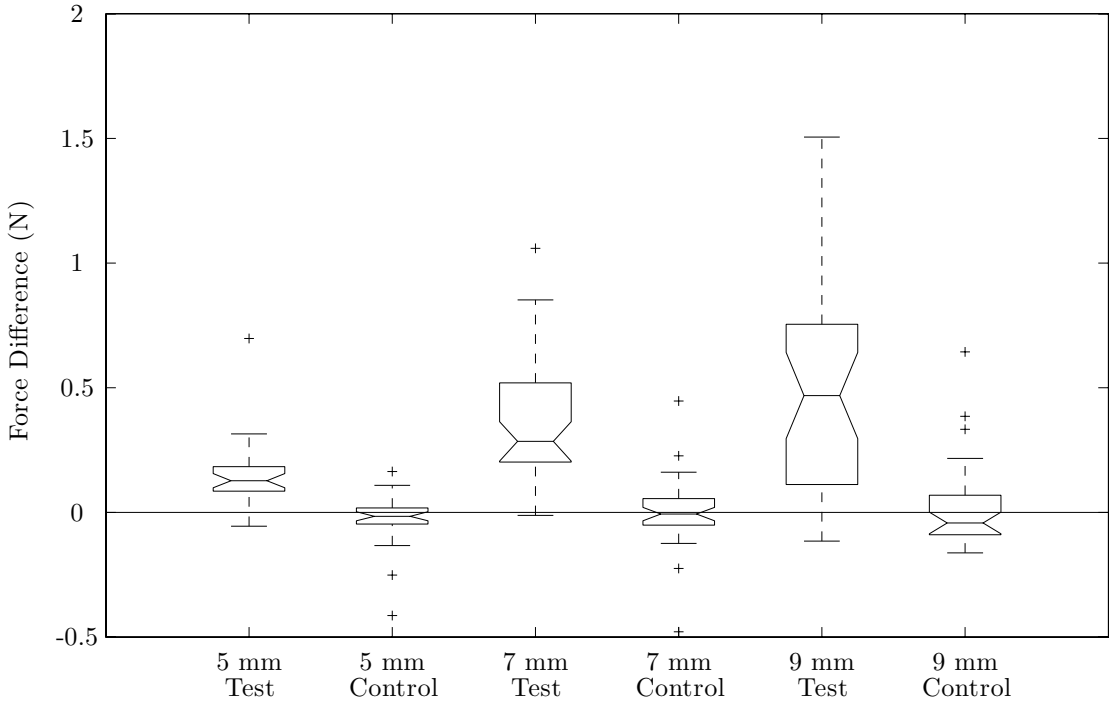

Figure 6: ΔF of the peak measurements from the variable-velocity experimental approach.

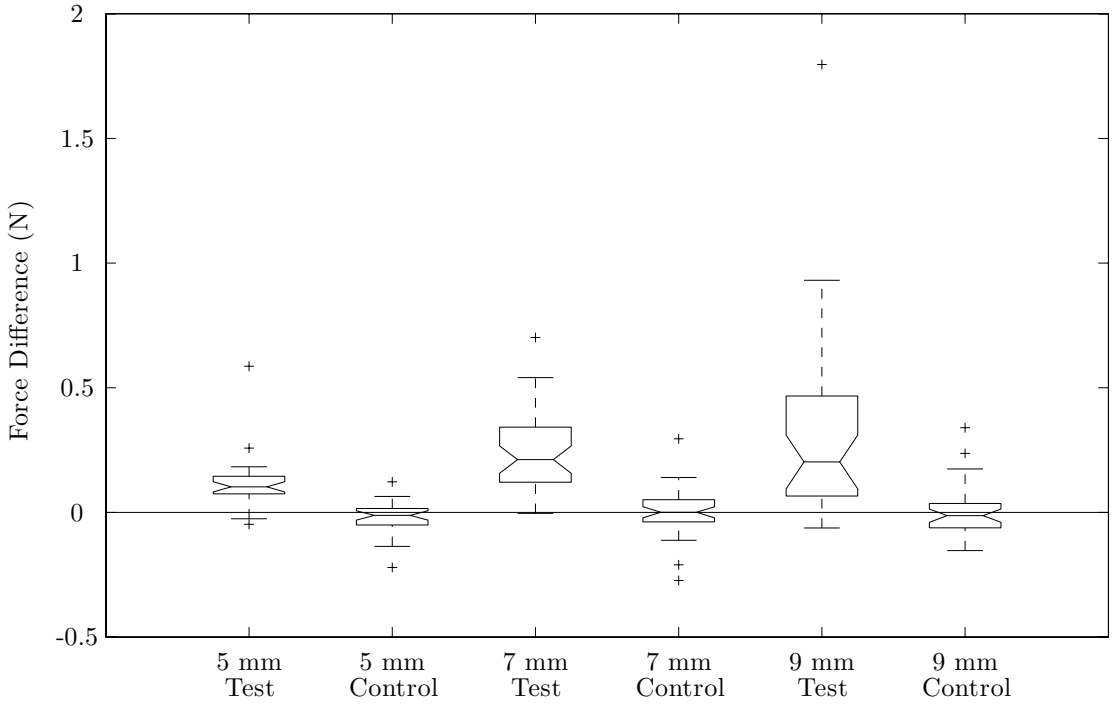

Figure 7: ΔF of the settled measurements from the variable-velocity experimental approach.

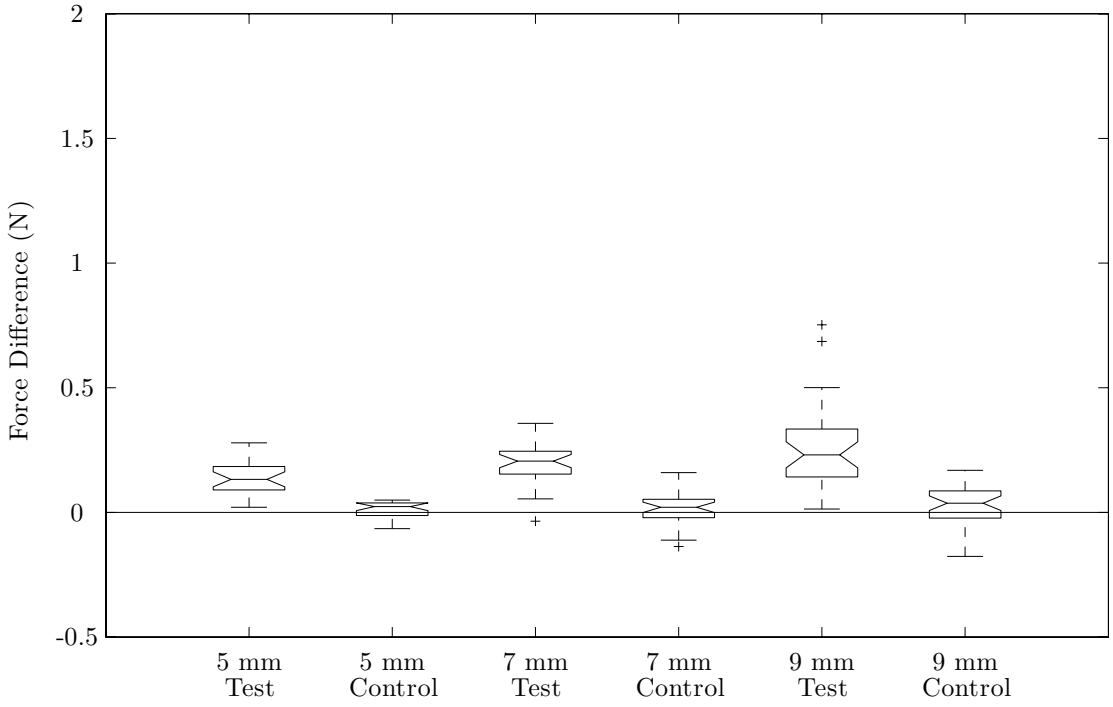

Figure 8: ΔF of the peak measurements from the constant-velocity experimental approach.

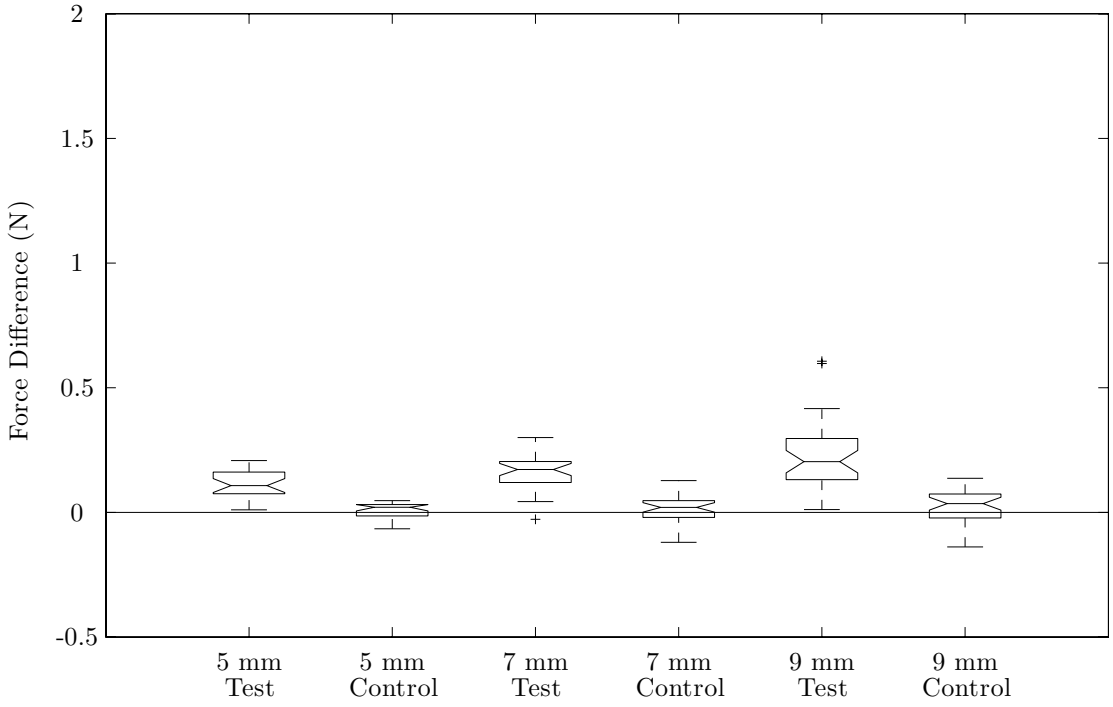

Figure 9: ΔF of the settled measurements from the constant-velocity experimental approach.

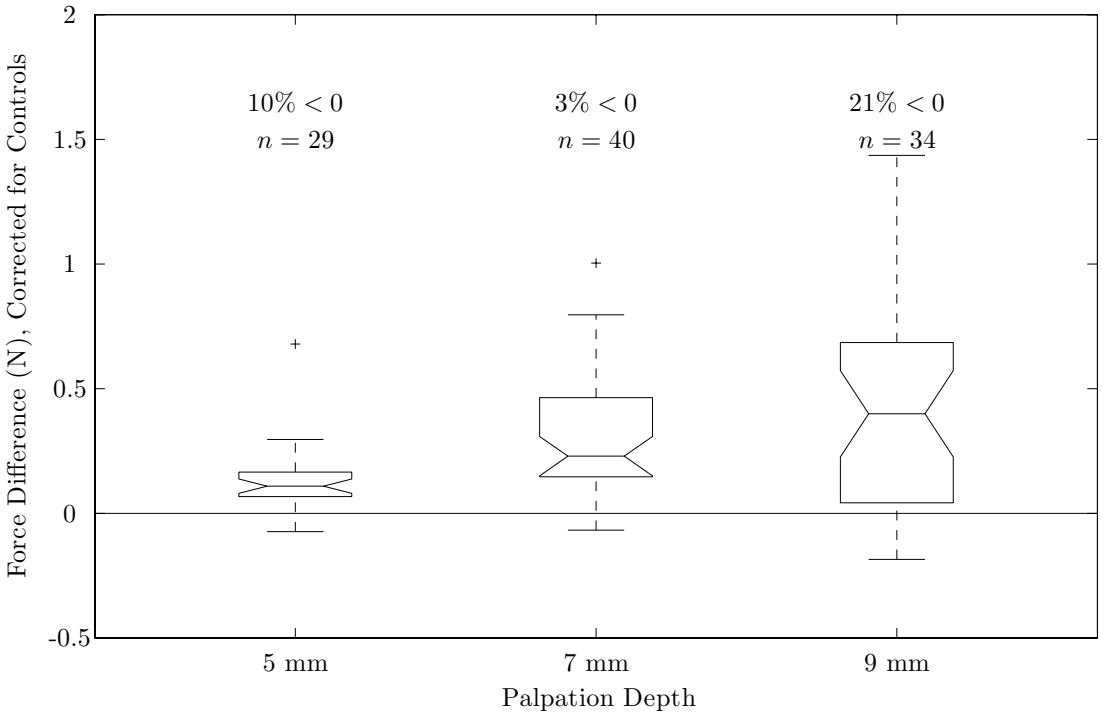

Figure 10: ΔF of the peak measurements from the variable-velocity experimental approach, corrected for the deviations in the associated control.

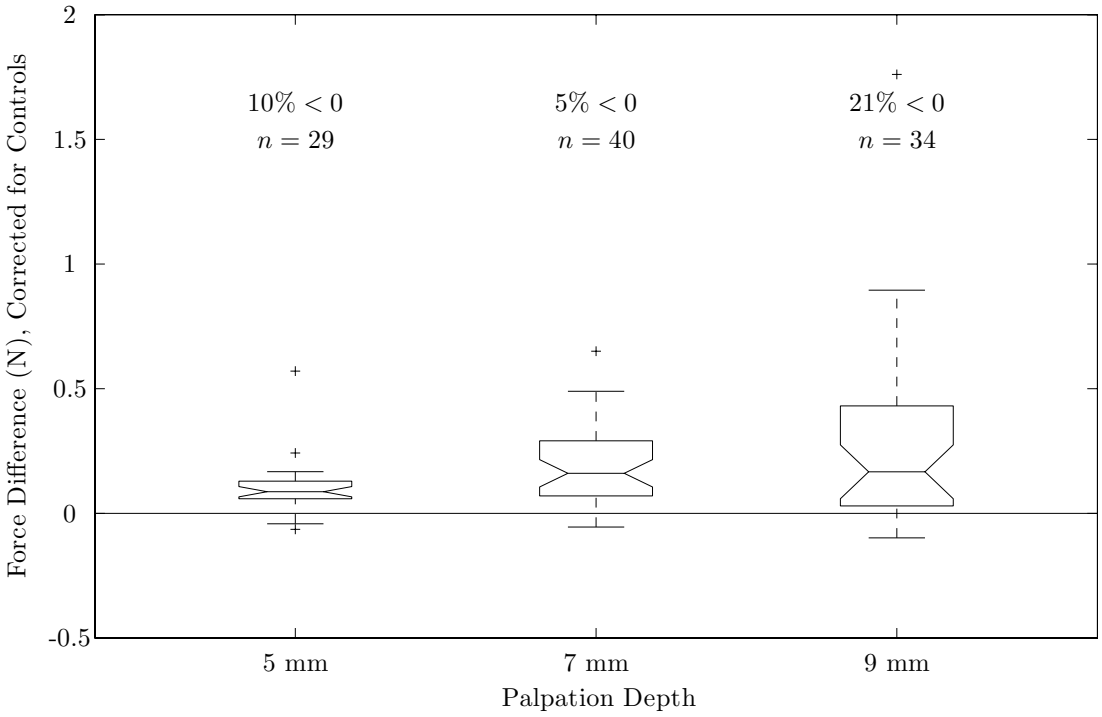

Figure 11: ΔF of the settled measurements from the variable-velocity experimental approach, corrected for the deviations in the associated control.

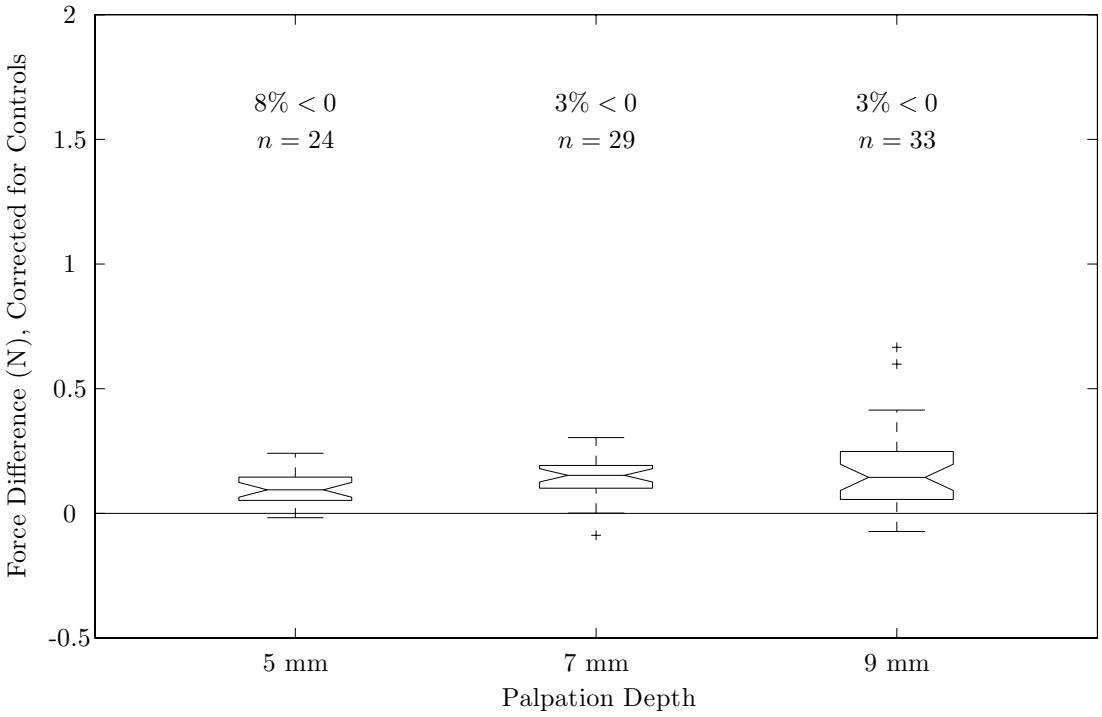

Figure 12: ΔF of the peak measurements from the constant-velocity experimental approach, corrected for the deviations in the associated control.

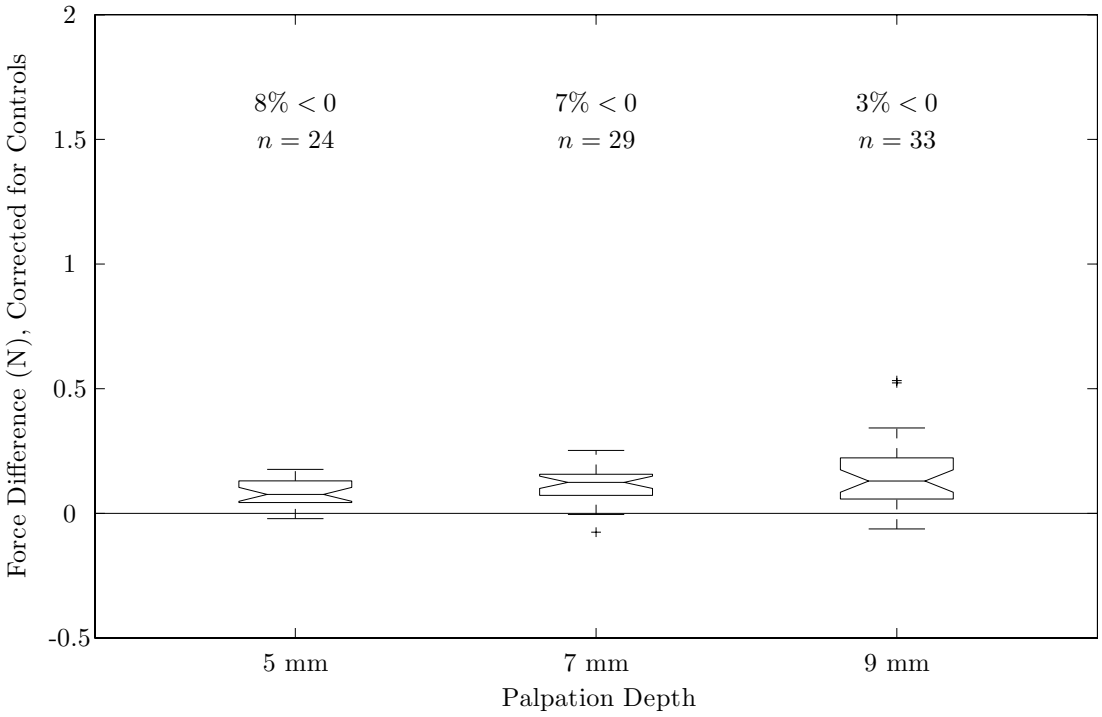

Figure 13: ΔF of the settled measurements from the constant-velocity experimental approach, corrected for the deviations in the associated control.